Mesoporous Materials

DOI: 10.1002/ange.201303353

A Resol-Assisted Co-Assembly Approach to Crystalline Mesoporous Niobia Spheres for Electrochemical Biosensing**

Wei Luo, Yuhui Li, Junping Dong, Jing Wei, Jiaqiang Xu, Yonghui Deng, and Dongyuan Zhao**

Ordered mesoporous materials have attracted considerable attention owing to their distinctive properties and great potential for applications in catalysis,[1–5] adsorption,[6–8] separation,[9,10] electrochemistry,[11–15] sensors,[16–19] and drug delivery.[20–23] As an important transition-metal oxide, niobium oxide is attracting more and more attention owing to its unique catalytic and electronic properties and applications in catalysis, sensing, electronic, and magnetic devices.[24–28] Design and synthesis of ordered mesoporous niobium oxides are important to improve their application performances, because the uniform and well-connected mesopores can facilitate the diffusion of guest molecules within frameworks and the high surface areas can offer abundant accessible active sites.

Solvent-evaporation-induced self-assembly (EISA) has been employed to synthesize various ordered mesoporous metal oxides by using various amphiphilic organic molecules as the template.[29–38] However, most of the mesoporous niobium oxides reported to date suffered some problems, including limited small pore size, low ordering of mesostructure, and unstable framework with low crystallinity. Interestingly, by using poly(isoprene-*block*-ethylene oxide) with high-molecular weight (ca. 33500 $g\,mol^{-1}$) as the template, Lee et al. recently have developed a combined assembly by soft and hard (CASH) method for synthesis of ordered mesoporous niobia with crystalline frameworks.[39] Similar to the typical EISA approach, the CASH method is sensitive to synthesis condition, and a slight fluctuation of environmental humidity can affect co-assembly process, resulting in poorly ordered mesostructures. Additionally, the EISA approach usually only leads to film-like or monolithic mesoporous materials that have unfavorable pore orientation (e.g. mesopores running parallel to their surface), limited pore connection and accessibility, thus impeding their applications in catalysis and sensor. Therefore, the exploration of new synthetic strategy for a facile and controllable synthesis of ordered mesoporous metal oxides with unique pore orientation is of high importance and great interest.

As a synthetic polymer oligomer, resol is soluble in most polar solvents (e.g. water, ethanol, THF) and has multiple phenolic hydroxy groups. It can self-polymerize into rigid phenolic formaldehyde (PF) resin upon heating. Resol has been used as good building block to co-assemble with amphiphilic block copolymers (e.g. Pluronic copolymers) by hydrogen bonding without strictly controlling over the synthetic conditions (e.g. solvent, humidity, solvent evaporation rate),[40–43] giving rise to ordered mesoporous PF resins, and even ordered mesoporous carbons after a further pyrolysis in inert atmospheres. Inspired by the unique properties of resol, we herein demonstrate a facile resol-assisted solvent evaporation induced self-assembly (RA-EISA) to synthesize ordered mesoporous niobium oxides. In this approach, the precursor solution containing THF solvent, acidic aqueous solution, resol, $NbCl_5$, and diblock copolymer PEO-*b*-PS was first allowed to slowly evaporate, and the resulting PF-Nb/PEO-*b*-PS composites were then heated at 100 °C for polymerization of phenolic resin. Subsequently, the composites were pyrolyzed in N_2 atmosphere at 350 and 550 °C, respectively, for removal of the copolymer templates and carbonization of PF and simultaneous crystallization of niobia. Finally, the obtained carbon-niobia composites were calcined at 400 °C in air to remove carbon species, giving rise to ordered mesoporous crystalline niobium oxides. The obtained mesoporous niobia materials have a unique spherical morphology with a diameter of 0.2–1.0 μm, large pore size (ca. 11.4 nm), high surface area (131 $m^2\,g^{-1}$) and pore volume (0.26 $cm^3\,g^{-1}$), and show excellent performance for loading hemoglobin (Hb) as an electrochemical sensor with a high sensitivity and fast response time.

Field-emission electron scanning electron microscopy (FE-SEM) images indicate that the as-made inorganic–organic PF-Nb/PEO-*b*-PS composites obtained by RA-EISA process after thermosetting at 100 °C consist of spherical particles with a diameter of 0.2–1.0 μm (Supporting Information, Figure S1a). Such a distinct spherical morphology has rarely been observed in typical EISA process, through which dense film-like organic–inorganic composites are usually obtained. After a further treatment in N_2 at 350 °C, black PF-Nb composites can be obtained owing to the partial carbonization of organic species. The PF-Nb composites

[*] W. Luo, Y. H. Li, J. Wei, Prof. Dr. Y. H. Deng, Prof. Dr. D. Y. Zhao
Department of Chemistry, Laboratory of Advanced Materials
Fudan University
Shanghai 200433 (China)
E-mail: yhdeng@fudan.edu.cn
dyzhao@fudan.edu.cn
Homepage: http://www.mesogroup.fudan.edu.cn/
Dr. J. P. Dong, Prof. Dr. J. Q. Xu
Department of Chemistry, College of Science, Shanghai University
Shanghai 200444 (China)

[**] This work was supported by the State Key 973 Program of the PRC (2012CB224805, 2013CB934104), NSF of China (61071040 and 21210004), the innovation Program of Shanghai Municipal Education Commission (13ZZ004), the Specialized Research Fund for the Doctoral Program of Higher Education of China (20120071110007), the Shanghai Rising Star Project of STCSM (12QH1400300) and Program for New Century Excellent Talents in University (NCET-12-0123).

Supporting information for this article is available on the WWW under http://dx.doi.org/10.1002/anie.201303353.

retained their spherical morphology (Figure S1b), and the porous structure can be clearly visible in the surface as a result of the selective removal of PEO-*b*-PS templates.[44,45] The highly ordered array of trenches with the feature of around 20 nm shown in the high-magnification FESEM image (Figure S1b, inset) implies a two-dimensional (2D) hexagonal mesostructure. After further carbonization of the composites in N_2 at 550 °C and calcination in air at 400 °C, both the spherical morphology and ordered mesostructure are retained (Figure 1 a,b), indicating that the mesoporous

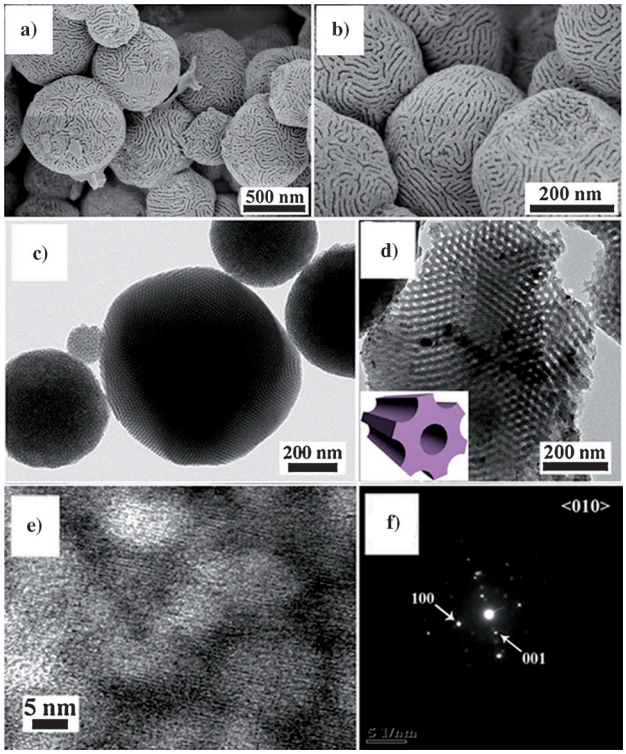

Figure 1. FESEM images of a, b) the mesoporous niobia spheres. TEM images of the mesoporous Nb_2O_5 spheres obtained c) before and d) after grinding. Inset in (d) is the structural model of mesopores. e) HRTEM image and f) the corresponding SAED.

niobia spheres have a good thermal stability. Compared to the mesoporous PF-Nb composites, the mesoporous niobia spheres have much rougher surfaces owing to the removal of the PF resin in the composites.

The small angle X-ray scattering (SAXS) pattern (Figure 2 a) of the as-made PF-Nb/PEO-*b*-PS composites shows three scattering peaks at q values of 0.228, 0.455, and 0.597 nm^{-1}, respectively, which can be indexed as the 100, 200, and 210 reflections of 2D hexagonal mesostructure with the space group *p6mm*. The unit cell parameter (a_0) is calculated to be 31.8 nm, indicative of a large unit of mesostructure. After a treatment at 350 °C under N_2 atmosphere, the PF-Nb composites also display three scatterings attributable to the ordered 2D hexagonal mesostructures (Figure 2 b) with a unit cell parameter of approximately 28.3 nm. After further pyrolysis at 550 °C in N_2 and then

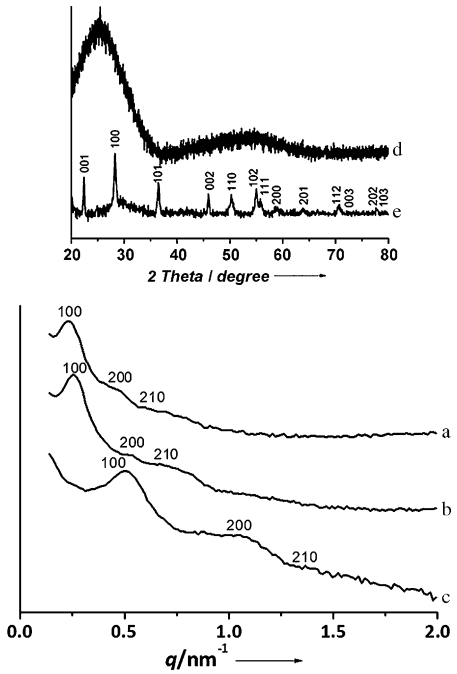

Figure 2. SAXS patterns of a) the as-made mesoporous PF-Nb/PEO-*b*-PS composites, b) the mesoporous PF-Nb composites after further thermal removal of templates under N_2, and c) the mesoporous niobia spheres. Inset: WA-XRD patterns of d) the mesoporous PF-Nb composites, and e) the mesoporous niobia spheres. Patterns are vertically offset for clarity

400 °C in air, the mesoporous niobia spheres exhibit similar SAXS patterns and a partially structural shrinkage because of the removal of carbon species and crystallization of niobia framework, indicating a stable mesostructure (Figure 2 c).

Transmission electron microscopy (TEM) observations show that the PF-Nb composites obtained after pyrolysis at 350 °C are spherical in shape (Figure S1c), and have regular arrays of mesopores with about 15 nm in size can also be clearly visible (Figure S1c, inset). To further investigate mesopore channels, the PF-Nb composites were slightly grinded for TEM observations. The fragment of the PF-Nb composites shows both 2D hexagonal arrays of mesopores and tubular channels viewed from the [100] and [110] directions, respectively (Figure S1d). The interlacing projections reveal that the mesopores are highly open and oriented in different directions. The energy dispersive X-ray spectroscopy (EDS) mapping images recorded on a single mesoporous PF-Nb composites show that the C, O ,and Nb elements are homogeneously distributed in the entire spheres (Figure S2). It suggests that the resol molecules can interact with the Nb precursors and co-assemble with PEO-*b*-PS molecules into mesostructured composite spheres. Similar to the mesoporous PF-Nb composites, the mesoporous niobia spheres show spherical morphology and ordered mesostructure, in good agreement with the SEM results. The diameter of the spheres ranges from around 200 nm to 1.0 μm (Figure 1 c). The ordered 2D hexagonal mesostructures viewed from [100] and [110] directions can be clearly observed in the TEM images of the grinded sample (Figure 1 d). The High reso-

lution TEM (HRTEM) image and corresponding selected-area electron diffraction (SAED) patterns of the mesoporous niobia sample (Figure 1e,f) further confirm a crystalline framework of the mesoporous niobia. The lattice fringes of niobia can be clearly observed around the mesopores, and the d-spacing is calculated to be 0.24 nm, corresponding to the (101) planes. These results indicate that the ordered mesoporous structure is retained after removing carbon species and frameworks crystallization.

Wide-angle XRD (WA-XRD) patterns of the mesoporous PF-Nb composites (Figure 2d) show broad diffraction peaks at 2θ of 25 and 55°, indicating an amorphous feature. After the crystallization at 550 °C and removal of the carbon at 400 °C, the mesoporous niobia materials show well-defined WA-XRD patterns with strong diffractions (Figure 2e), indicating the formation of crystalline niobia (JCPDS No. 07-0061). The nitrogen sorption isotherms (Figure 3a) of the

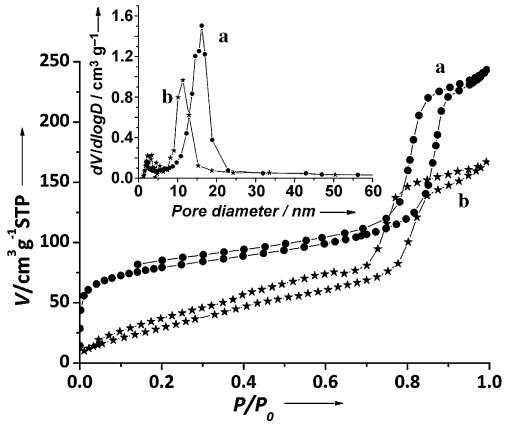

Figure 3. N_2 adsorption–desorption isotherms and the pore size distribution curves (inset) of a) the mesoporous PF-Nb composite spheres obtained after the pyrolysis at 350 °C in N_2; b) the mesoporous Nb_2O_5 spheres.

mesoporous PF-Nb composites show typical type-IV curves with H_1 hysteresis loop with a sharp capillary condensation step in the relative pressure (P/P_0) of 0.80–0.90, which is typical for 2D hexagonal mesoporous materials with uniform and large pore size. The pore diameter is about 16.2 nm as indicated in the pore size distributions derived from the adsorption branch of the isotherms by using Barrett-Joyner-Halenda (BJH) model (inset in Figure 3a). The pore wall thickness of the mesoporous PF-Nb composites is calculated to be about 12.1 nm. The BET surface area and total pore volume are approximately 279 $m^2 g^{-1}$ and 0.32 $cm^3 g^{-1}$, respectively. Similar to the PF-Nb composites, the mesoporous crystalline Nb_2O_5 displays type-IV curves with H_1 hysteresis loop (Figure 3b). Interestingly, as shown in the pore size distribution curves (inset in Figure 3b), the mesoporous crystalline Nb_2O_5 shows a bimodal pores. The large pore centered at approximately 11.4 nm is probably from PEO-*b*-PS molecules, and the small one at about 3.5 nm is mainly attributed the removal to carbon species in the carbon–Nb composites after the calcination in air at 400 °C, indicating that PF-derived carbon species are well distributed in the niobia matrix in hybrid nanocomposites. The BET surface area and pore volume of the mesoporous Nb_2O_5 spheres drop to around 131 $m^2 g^{-1}$ and 0.26 $cm^3 g^{-1}$, respectively, as a result of the crystallization of the frameworks.

The ordered mesoporous niobia spheres can be readily synthesized from our RA-EISA approach in a broad humidity range from 30 to even 80 %. The $NbCl_5$/resol weight ratio is crucial for the ordered mesoporous niobia spheres. A series of control experiments reveal that the optimized ratio is 1–3:1. Using excess resol, ordered mesoporous PF-Nb composites with similar spherical morphology and mesostructure can be obtained, but upon the removal of PF-derived carbon species by calcination in air, the mesostructures are unstable and collapsed because of insufficient cross-linking in the niobia frameworks. When the $NbCl_5$/resol ratio is too high or without the addition of resol, the ordered mesostructure from the self-assembly process could not be formed, because without the assistance of the resol the interaction between the template and Nb source is too weak. The mesoporous niobia synthesized without resol after calcination are composed of large particles with disordered structures (Figure S3), further suggesting that the resol assistance is crucial for the formation of an ordered Nb_2O_5 mesostructure. Although previous work shows that mesoporous carbon–TiO_2, carbon–Al_2O_3, and carbon–WO_3 composites[46–48] can be synthesized by using resol as the carbon source and block copolymer as the templates, they failed to convert into the corresponding mesoporous metal oxides because of structure collapse during calcination.

Based on the above results, we propose a resol-assisted solvent evaporation induced self-assembly for the formation of the large-pore ordered mesoporous niobia spheres (Figure 4). At the first stage, the water-insoluble PEO-*b*-PS dissolves well in acidic THF/H_2O/resol/$NbCl_5$ solution with a very high volume ratio of THF (90 %). Along with the fast evaporation of THF at 50 °C, the hydrophobic PS segments of the block copolymers tend to aggregate to form rod-like micelles with PS block as a core surrounded by PEO shells. Meanwhile, since the resol precursors can interact with the PEO segments of PEO-*b*-PS templates by hydrogen-bonding interactions and associate with inorganic Nb^{5+} species by chelating,[49] the PEO domains are decorated by resol and Nb^{5+} species, forming cylindrical core–shell micelles with rod-like PS microdomains covered by the resol/Nb^{5+} composites (Figure 4 Step 1). Therefore, the resol molecules serve as a glue which binds Nb^{5+} species around the PEO domains, preventing the macroscopic phase separation of PEO-*b*-PS and Nb^{5+} species. During the evaporation, the cylindrical core–shell composites can gradually pack together to form mesostructures. As THF further evaporates, PEO-*b*-PS/resol/$NbCl_5$ composites become more insoluble because of the strong hydrophobic nature of the PS segments, and thus the flexible core–shell composite micelles tend to bend and aggregate as a result of the interfacial force of water and THF, to form composite particles with irregular shapes (Step 2). Finally, a phase separation of the composites occurs from the water-rich liquid phase, and the composite micelles can further be packed to form spherical particles on the interface of the water-rich solution to reduce curvature energy (Step 3).

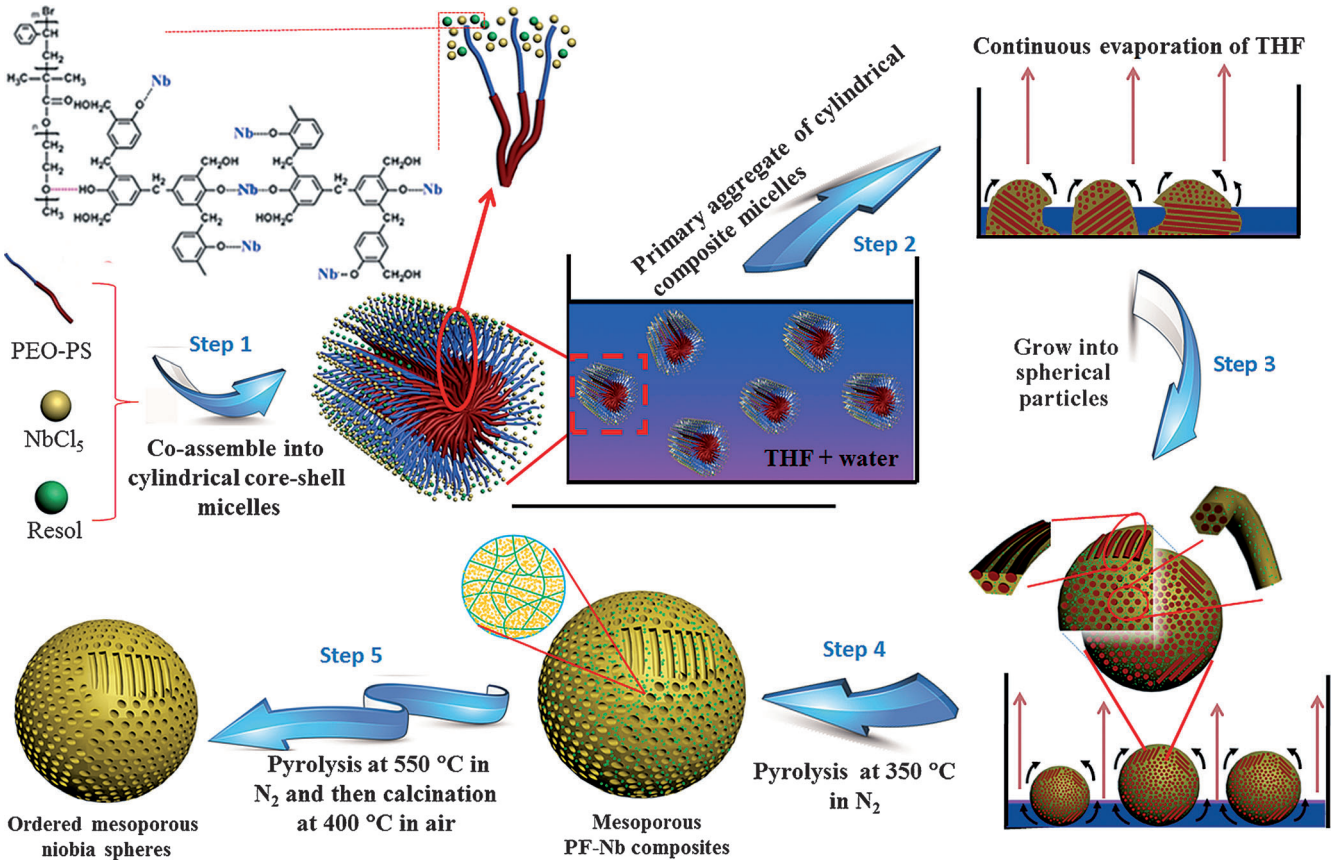

Figure 4. The formation process of the ordered mesoporous Nb_2O_5 spheres by the resol-assisted evaporation-induced self-assembly approach. Step 1: the formation of cylindrical composite micelles with a core of PS blocks and a shell of PEO segments decorated by the resol and Nb^{5+} species through hydrogen bonding interactions and chelation; Step 2: the formation of the composite particles with irregular shape by the bending and aggregation of flexible core–shell composite micelles; Step 3: the formation of the mesostructured composite spheres on the surface of the water-rich liquid phase by the aggregation of the cylindrical composite micelles to reduce interface curvature energy; Step 4: the formation of the mesoporous PF-Nb composites by the polymerization of resols at 100 °C and then heating at 350 °C in N_2 to selectively decompose the template. Step 5: the formation of ordered mesoporous niobia spheres with crystalline frameworks by further heating at 550 °C in N_2 and then calcination at 400 °C in air to remove the PF-derived carbon which supports the porous structure and prevents the collapse of the framework during crystallization.

During the evaporation and phase separation, the hexagonal mesostructure of the resol/Nb_2O_5/PS-*b*-PEO composites can further re-organize into a highly regular arrangement. By the subsequent heating at 100 °C, the resol molecules thermally polymerize into PF polymers, which fixes the composite spheres and the niobia oligomers can be further condensed, forming a "reinforced-concrete" framework structure. By pyrolysis at 350 °C in N_2, the PEO-*b*-PS templates are selectively decomposed, leaving behind uniform mesopores in the PF-Nb composites with well-retained spherical morphology (Step 4). During the further treatment at 550 °C in nitrogen, niobia species can be crystallized without the structure collapse as a result of the support of the PF-derived carbon. At last, ordered mesoporous niobia with a spherical morphology and large pore sizes can be obtained by calcination at 400 °C in air to remove the carbon species (Step 5).

Haemoglobin (Hb) is nearly spherical with molecular size of $5.0 \times 5.5 \times 6.5$ nm. The relative large pores (ca. 11.4 nm) of the mesoporous Nb_2O_5 obtained are wide enough to accommodate Hb molecules. Hydrogen peroxide (H_2O_2) is a primary product of the oxidation for some important biomolecules in the presence of the highly selective oxidase, the fabrication of biosensors based on H_2O_2 is highly important. In this study, we investigated the performance of the mesoporous niobia spheres as a matrix for Hb immobilization and electrochemical biosensing to H_2O_2 (see Supporting Information for experimental details). No clear redox waves were observed by cyclic voltammetry at the Nb_2O_5 modified electrode (Figure S4), indicating that pristine Nb_2O_5 is an electro-inactive matrix. After immobilization of Hb, a pair of ill-defined redox waves appear at $-0.247/-0.135$ V (Figure S4), which are attributed to the HB-heme $Fe^{III} + H^+ + e^- \rightleftarrows$HB-heme Fe^{II} redox couple. This is an indication of the direct electron transfer between Hb and electrode surface. Figure S5 A illustrates the cyclic voltammograms of the mesoporous Nb_2O_5–HB biosensor in the absence and presence of the different concentrations of H_2O_2. As the different amounts of H_2O_2 are added to the buffer solution (pH 7.0), cathodic peak currents gradually increase, indicating that the biosensor can catalyze the reduction of H_2O_2. The amperometric response of the Nb_2O_5–HB biosensor was investigated by successive

additions of H_2O_2. When different concentrations of H_2O_2 are added into the pH 7.0 buffer solution, the reductive currents rose steeply to reach a stable value (Figure S5B). The biosensor can achieve 95% of the steady-state current within 5 s, indicating a fast response of the biosensor. The amperometric currents increase linearly with H_2O_2 concentration in both the low concentration range of 5.0–60 μM (Figure S5C) and high concentration of 80 μM–11 mM (Figure S5D) with good linear regression equations. As a result, a biosensor based on hydrogen peroxide was successfully fabricated by immobilizing Hb on the spherical mesoporous Nb_2O_5 with large pores. A sensor based on Hb-Au-modified SBA-15 has been reported with a linear response range of 5.0 μm–11 mM, our material gives a better performance with a wider linear response range.[50]

In summary, a resol-assisted solvent evaporation induced self-assembly has been demonstrated for the first time to synthesize large-pore mesoporous niobia spheres with a 2D hexagonal mesostructure by using a high molecular weight PEO-*b*-PS copolymer as a structure-directing agent, resol and $NbCl_5$ as the precursors, THF as a solvent, and adding small amount of HNO_3. With the assistance of the resol precursor, ordered mesostructured PF-niobia composites can be obtained in a wide range of conditions without the need to careful control the humidity; the hydrolysis and condensation of the niobium species can be slowed down by the PF matrix. The ordered mesoporous niobia spheres obtained have a diameter of 0.2–1.0 μm, uniform large mesopores of approximately 11.4 nm, relatively high surface areas of around 131 $m^2 g^{-1}$, and pore volumes of about 0.26 $cm^3 g^{-1}$. A novel biosensor was fabricated by immobilization of Hb in the mesoporous niobia spheres. It exhibits excellent electrochemical sensing of H_2O_2 with a high sensitivity and fast response time as a result of the short mass diffusion length, large pores size, and high surface area.

Received: April 20, 2013
Revised: June 6, 2013
Published online: August 13, 2013

Keywords: biosensor · block copolymers · mesoporous materials · niobium · resol

[1] A. Corma, *Chem. Rev.* **1997**, *97*, 2373 – 2420.
[2] Y. Wan, D. Y. Zhao, *Chem. Rev.* **2007**, *107*, 2821 – 2860.
[3] F. Goettmann, A. Fischer, M. Antonietti, A. Thomas, *Angew. Chem.* **2006**, *118*, 4579 – 4583; *Angew. Chem. Int. Ed.* **2006**, *45*, 4467 – 4471.
[4] C. Tagusagawa, A. Takagaki, A. Iguchi, K. Takanabe, J. N. Kondo, K. Ebitani, S. Hayashi, T. Tatsumi, K. Domen, *Angew. Chem.* **2010**, *122*, 1146 – 1150; *Angew. Chem. Int. Ed.* **2010**, *49*, 1128 – 1132.
[5] Y. H. Deng, Y. Cai, Z. K. Sun, J. Liu, C. Liu, J. Wei, W. Li, C. Liu, Y. Wang, D. Y. Zhao, *J. Am. Chem. Soc.* **2010**, *132*, 8466 – 8473.
[6] A. Sayari, S. Hamoudi, Y. Yang, *Chem. Mater.* **2005**, *17*, 212 – 216.
[7] Y. H. Deng, D. W. Qi, C. H. Deng, X. M. Zhang, D. Y. Zhao, *J. Am. Chem. Soc.* **2008**, *130*, 28 – 29.
[8] Z. K. Sun, Y. H. Deng, J. Wei, D. Gu, B. Tu, D. Y. Zhao, *Chem. Mater.* **2011**, *23*, 2176 – 2184.
[9] G. S. Armatas, M. G. Kanatzidis, *Nat. Mater.* **2009**, *8*, 217 – 222.
[10] T. Y. Ma, H. Li, A. N. Tang, Z. Y. Yuan, *Small* **2011**, *7*, 1827 – 1837.
[11] P. A. Nelson, J. M. Elliott, G. S. Attard, J. R. Owen, *Chem. Mater.* **2002**, *14*, 524 – 529.
[12] H. Zhou, S. Zhu, M. Hibino, I. Honma, M. Ichihara, *Adv. Mater.* **2003**, *15*, 2107 – 2111.
[13] R. L. Liu, Y. F. Shi, Y. Wan, Y. Meng, F. Q. Zhang, D. Gu, Z. X. Chen, B. Tu, D. Y. Zhao, *J. Am. Chem. Soc.* **2006**, *128*, 11652 – 11662.
[14] X. P. Dong, W. H. Shen, J. L. Gu, L. M. Xiong, Y. F. Zhu, H. Li, J. L. Shi, *J. Phys. Chem. B* **2006**, *110*, 6015 – 6019.
[15] G. X. Wang, H. Liu, J. Horvat, B. Wang, S. Z. Qiao, J. S. Park, H. J. Ahn, *Chem. Eur. J.* **2010**, *16*, 11020 – 11027.
[16] M. E. Gimon-Kinsel, K. J. Balkus, *Microporous Mesoporous Mater.* **1999**, *28*, 113 – 123.
[17] E. Rossinyol, A. Prim, E. Pellicer, J. Arbiol, F. Hernandez-Ramirez, F. Peiró, A. Cornet, J. R. Morante, L. A. Solovyov, B. Z. Tian, T. Bo, D. Y. Zhao, *Adv. Funct. Mater.* **2007**, *17*, 1801 – 1806.
[18] E. Z. Lee, Y. S. Jun, W. H. Hong, A. Thomas, M. M. Jin, *Angew. Chem.* **2010**, *122*, 9900 – 9904; *Angew. Chem. Int. Ed.* **2010**, *49*, 9706 – 9710.
[19] A. Prim, E. Pellicer, E. Rossinyol, F. Peiró, A. Cornet, J. R. Morante, *Adv. Funct. Mater.* **2007**, *17*, 2957 – 2963.
[20] C. Y. Lai, B. G. Trewyn, D. M. Jeftinija, K. Jeftinija, S. Xu, S. Jeftinija, V. S. Y. Lin, *J. Am. Chem. Soc.* **2003**, *125*, 4451 – 4459.
[21] Y. F. Zhu, J. L. Shi, W. H. Shen, X. P. Dong, J. W. Feng, M. L. Ruan, Y. S. Li, *Angew. Chem.* **2005**, *117*, 5213 – 5217; *Angew. Chem. Int. Ed.* **2005**, *44*, 5083 – 5087.
[22] I. I. Slowing, B. G. Trewyn, S. Giri, Lin, V. S.-Y. Lin, *Adv. Funct. Mater.* **2007**, *17*, 1225 – 1236.
[23] H. F. Bao, J. P. Yang, Y. Huang, Z. P. Xu, N. Hao, Z. X. Wu, G. Q. Lu, D. Y. Zhao, *Nanoscale* **2011**, *3*, 4069 – 4073.
[24] K. Tanabe, *Appl. Catal. A* **1996**, *133*, 191 – 218.
[25] S. H. Chai, H. P. Wang, Y. Liang, B. Q. Xu, *J. Catal.* **2007**, *250*, 342 – 349.
[26] D. Rosenfeld, P. E. Schmid, S. Széles, F. Lévy, V. Demarne, A. Grisel, *Sens. Actuators B* **1996**, *37*, 83 – 89.
[27] I. T. Weber, R. Andrade, E. R. Leite, E. Longor, *Sens. Actuators B* **2001**, *72*, 180 – 183.
[28] B. Varghese, S. C. Haur, C. T. Lim, *J. Phys. Chem. C* **2008**, *112*, 10008 – 10012.
[29] D. M. Antonelli, J. Y. Ying, *Angew. Chem.* **1996**, *108*, 461 – 464; *Angew. Chem. Int. Ed. Engl.* **1996**, *35*, 426 – 430.
[30] T. Sun, J. Y. Ying, *Angew. Chem.* **1998**, *110*, 690 – 693; *Angew. Chem. Int. Ed.* **1998**, *37*, 664 – 667.
[31] P. D. Yang, D. Y. Zhao, D. I. Margolese, B. F. Chmelka, G. D. Stucky, *Nature* **1998**, *396*, 152 – 155.
[32] P. D. Yang, D. Y. Zhao, D. I. Margolese, B. F. Chmelka, G. D. Stucky, *Chem. Mater.* **1999**, *11*, 2813 – 2826.
[33] B. Z. Tian, X. Y. Liu, B. Tu, C. Z. Yu, J. Fan, L. M. Wang, S. H. Xie, G. D. Stucky, D. Y. Zhao, *Nat. Mater.* **2003**, *2*, 159 – 163.
[34] O. Sel, D. Kuang, M. Thommes, B. Smarsly, *Langmuir* **2006**, *22*, 2311 – 2322.
[35] T. Brezesinski, A. Fischer, K. i. limura, C. Sanchez, D. Grosso, M. Antonietti, B. M. Smarsly, *Adv. Funct. Mater.* **2006**, *16*, 1433 – 1440.
[36] D. Fattakhova-Rohlfing, M. Wark, T. Brezesinski, B. M. Smarsly, J. Rathousky, *Adv. Funct. Mater.* **2007**, *17*, 123 – 132.
[37] Y. H. Deng, J. Wei, Z. K. Sun, D. Y. Zhao, *Chem. Soc. Rev.* **2013**, *42*, 4054 – 4070.
[38] J. Wei, Q. Yue, Z. K. Sun, Y. H. Deng, D. Y. Zhao, *Angew. Chem.* **2012**, *124*, 6253 – 6257; *Angew. Chem. Int. Ed.* **2012**, *51*, 6149 – 6153.
[39] J. W. Lee, O. M. Christopher, S. C. Warren, M. Kamperman, F. J. Disalvo, U. Wiesner, *Nat. Mater.* **2008**, *7*, 222 – 228.

[40] Y. H. Deng, T. Yu, Y. Wan, Y. F. Shi, Y. Meng, D. Gu, L. J. Zhang, Y. Huang, C. Liu, X. J. Wu, D. Y. Zhao, *J. Am. Chem. Soc.* **2007**, *129*, 1690 – 1697.
[41] Y. Meng, D. Gu, F. Q. Zhang, Y. F. Shi, H. F. Yang, Z. Li, C. Z. Yu, B. Tu, D. Y. Zhao, *Angew. Chem.* **2005**, *117*, 7215 – 7221; *Angew. Chem. Int. Ed.* **2005**, *44*, 7053 – 7059.
[42] Y. H. Deng, Y. Cai, Z. K. Sun, D. Gu, J. Wei, W. Li, X. H. Guo, J. P. Yang, D. Y. Zhao, *Adv. Funct. Mater.* **2010**, *20*, 3658 – 3665.
[43] J. Wei, D. D. Zhou, Z. K. Sun, Y. H. Deng, Y. Y. Xia, D. Y. Zhao, *Adv. Funct. Mater.* **2013**, *23*, 2322 – 2328.
[44] J. Wei, H. Wang, Y. H. Deng, Z. K. Sun, L. Shi, B. Tu, M. Luqman, D. Y. Zhao, *J. Am. Chem. Soc.* **2011**, *133*, 20369 – 20377.
[45] Q. Yue, M. H. Wang, J. Wei, Y. H. Deng, T. Y. Liu, R. C. Che, B. Tu, D. Y. Zhao, *Angew. Chem.* **2012**, *124*, 10514 – 10518; *Angew. Chem. Int. Ed.* **2012**, *51*, 10368 – 10372.
[46] R. L. Liu, Y. J. Ren, Y. F. Shi, F. Zhang, L. J. Zhang, B. Tu, D. Y. Zhao, *Chem. Mater.* **2008**, *20*, 1140 – 1146.
[47] C. Jo, J. Hwang, H. Song, A. H. Dao, Y. T. Kim, S. H. Lee, S. W. Hong, S. Yoon, J. Lee, *Adv. Funct. Mater.* **2013**, DOI: 10.1002/adfm.201202682.
[48] J. M. Xu, A. Q. Wang, X. D. Wang, D. S. Su, T. Zhang, *Nano Res.* **2011**, *4*, 50 – 60.
[49] Z. K. Sun, B. Sun, M. H. Qiao, J. Wei, Y. Qin, C. Wang, Y. H. Deng, S. Kaliaguine, D. Y. Zhao, *J. Am. Chem. Soc.* **2012**, *134*, 17653 – 17660.
[50] Y. Z. Xian, Y. Xian, L. H. Zhou, F. H. Wu, Y. Ling, L. T. Jin, *Electrochem. Commun.* **2007**, *9*, 142 – 148.